Supporting Information

Efficient photocatalytic hydrogen evolution and CO_2 reduction by $HfSe_2/GaAs_3$ and $ZrSe_2/GaAs_3$ heterostructures with direct Z-schemes

Xue-Qing Wan, Chuan-Lu Yang*, Mei-shan Wang, and Xiao-Guang Ma

School of Physics and Optoelectronic Engineering, Ludong University, Yantai 264025, China

1. The geometrical configurations and electronic properties of the monolayers and heterostructures

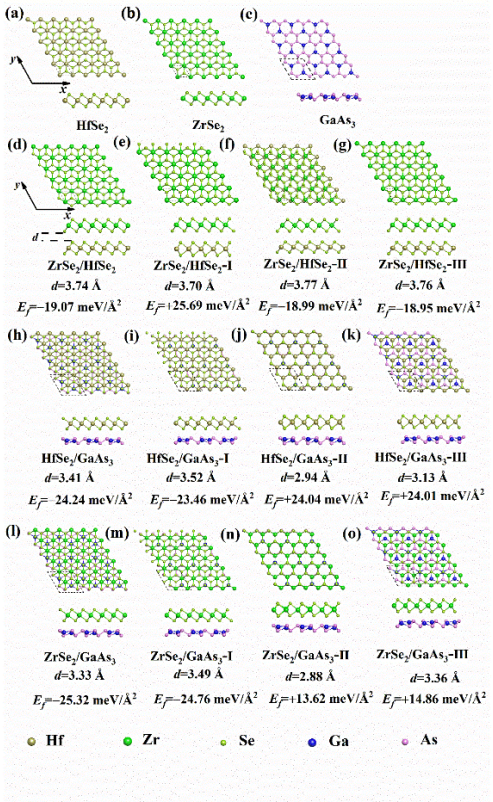

Fig. S1 The top and side views of the monolayers. (a)-(c), the $HfSe_2$, $ZrSe_2$, and $GaAs_3$ monolayers. The top views, side views, formation energies (E_f) and interlayer distances (d) of the heterostructures. (e)-(o), the $ZrSe_2/HfSe_2$, $ZrSe_2/HfSe_2$-I, $ZrSe_2/HfSe_2$-II, $ZrSe_2/HfSe_2$-III, $HfSe_2/GaAs_3$, $HfSe_2/GaAs_3$-I, $HfSe_2/GaAs_3$-II, $HfSe_2/GaAs_3$-III, $ZrSe_2/GaAs_3$, $ZrSe_2/GaAs_3$-I, $ZrSe_2/GaAs_3$-II and $ZrSe_2/GaAs_3$-III heterostructures.

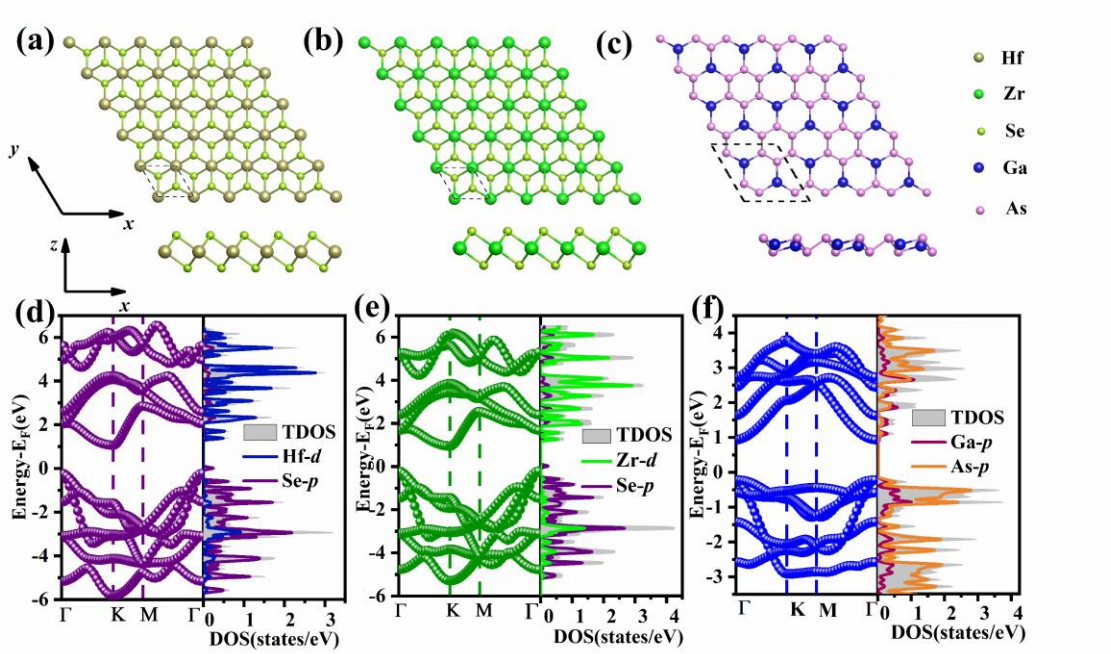

Fig. S2. The geometrical structures and the band structures of the (a) (d)$HfSe_2$, (b) (e) $ZrSe_2$ and (c) (f) $GaAs_3$ monolayers. The Fermi level is set to zero.

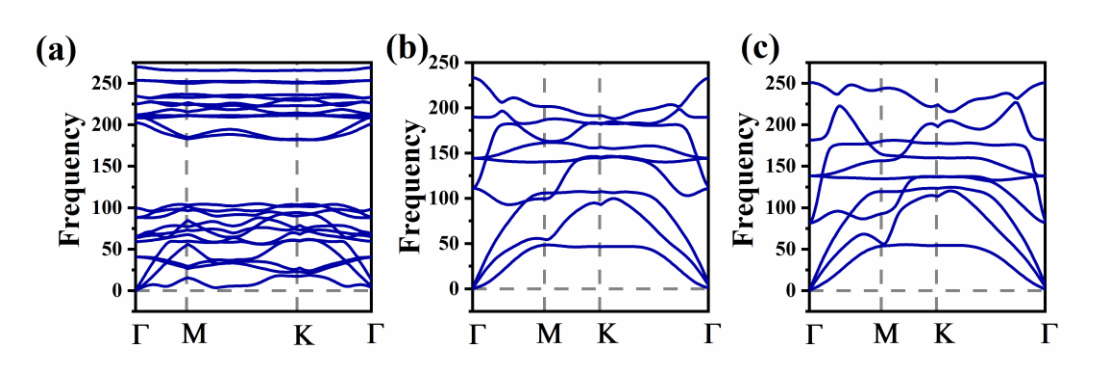

Fig. S3. The phonon dispersions of considered monolayers. (a) $GaAs_3$, (b) $HfSe_2$ and (c) $ZrSe_2$.

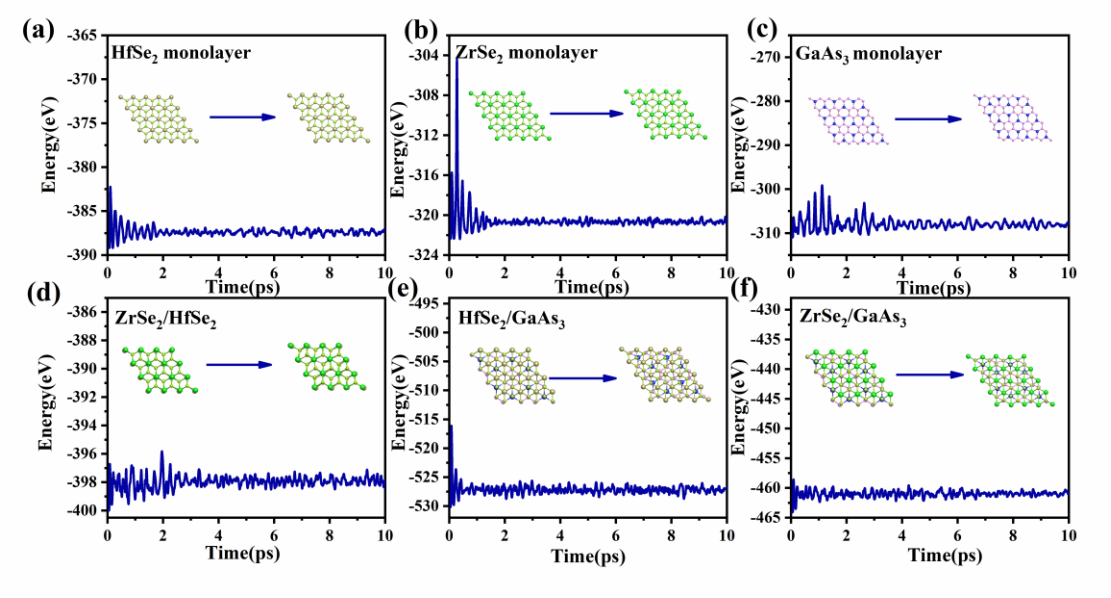

Fig. S3. The AIMD simulation results in a temperature of 300 K for the considered structures. (a) $HfSe_2$, (b) $ZrSe_2$, (c) $GaAs_3$, (d)$ZrSe_2/HfSe_2$, (e) $HfSe_2/GaAs_3$ and (f) $ZrSe_2/GaAs_3$.

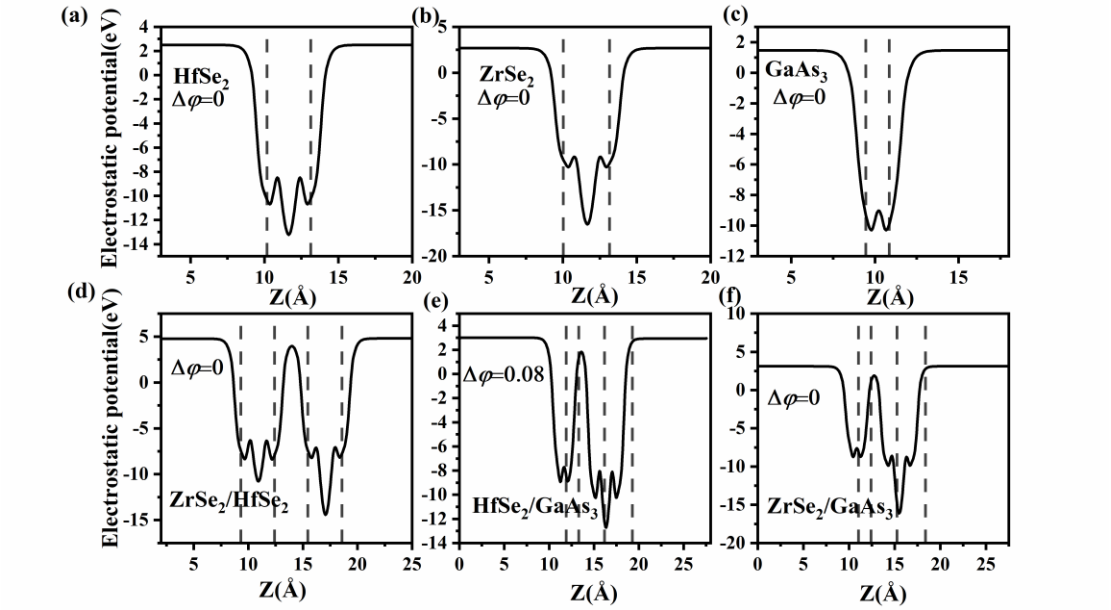

Fig. S5. The electrostatic potentials and the vacuum levels of the monolayers and the considered heterostructures. (a) $HfSe_2$, (b) $ZrSe_2$, (c) $GaAs_3$, (d) $HfSe_2/GaAs_3$, (f) $HfSe_2/GaAs_3$ and (g)$ZrSe_2/GaAs_3$.

Table. S1. The lattice constants, bandgaps, CBMs and VBMs calculated by HSE06 for $HfSe_2$, $ZrSe_2$ and $GaAs_3$ monolayers.

Monolayer	a (Å)	a (Å) (Exp./Cal.)	E_g(eV)	E_g(eV) (Exp./Cal.)	CBM (eV)	VBM (eV)
$HfSe_2$	3.73	3.78[1],3.70[2]	1.28	1.10[1],1.30[3]	-4.80	-6.09
$ZrSe_2$	3.76	3.77[4,5]	1.15	1.20[6],1.18[7]	-4.99	-6.15
$GaAs_3$	7.52	-----	1.16	-----	-4.26	-5.42

2. Details and calculational results of the carrier mobility

We calculated the carrier mobility of the three monolayers using the deformation potential (DP) theory 错误!未找到引用源。. The equation is [8-11]

$$\mu = \frac{2e\hbar^3 C}{3k_B T|m^*|^2 E_d^2} \quad (1)$$

Where the carrier mobility μ depends on the elastic modulus C, effective mass m^*, and deformation potential constant E_d. e, $\hbar$, k_B, and T are the electron charge, the reduced Planck constant, the Boltzmann constant, T is the temperature was set as 300 K. C, m^*, E_d, defined as $C = \frac{1}{S_0}\frac{\partial^2 E}{\partial \varepsilon^2}$, $\frac{1}{m^*} = \frac{1}{\hbar}\frac{\partial^2 E(k)}{\partial k^2}$, $E_d = \frac{\partial E_{edge}}{\partial \varepsilon}$, respectively. For the above equation C, m^*, E_d, where ε is the ratio of lattice parameter under the uniaxial strain along x or y direction on the rectangle cell, E is the total energy of the monolayer under uniaxial strains, S_0 is the area of the monolayer, and $E(k)$ is the energy corresponding to k, k is the wave vector. E_{edge} is the energy of the band edge position calculated by HSE06. The detailed results are shown in Fig. S6–S8†.

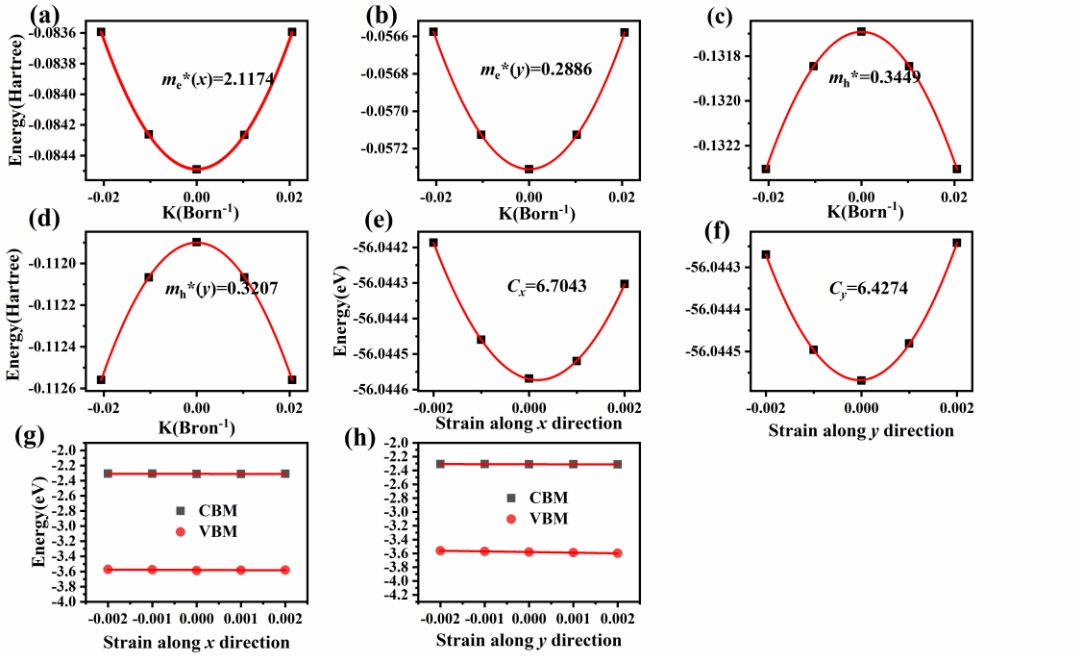

Fig. S6. Fitting curve of elastic constant (C), deformation potential constant (E_d), and effective mass (m*) of $HfSe_2$ monolayer. (a) and (b) are the m* fitting curves of the electrons along x and y directions, respectively. (c) and (d) are the m* fitting curves of the holes along x and y directions, respectively. (e) and (f) are the fitting curves of C along the x and y directions, respectively. (g) and (h) are the fitting curves of E_d along x and y directions, respectively.

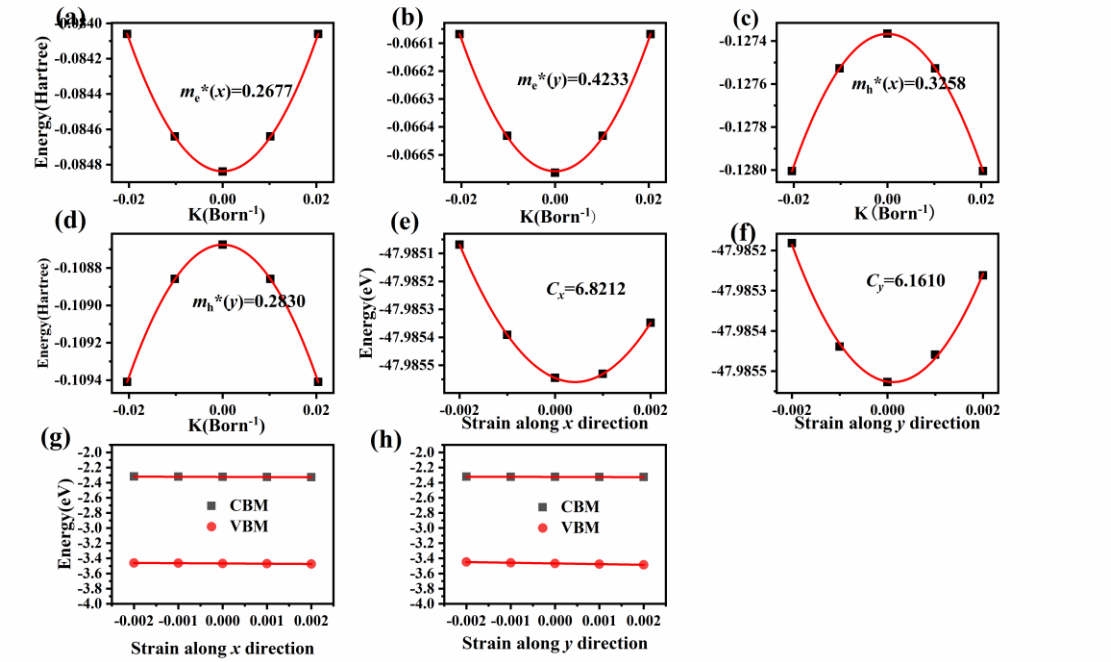

Fig. S7. Fitting curve of elastic constant (C), deformation potential constant (E_d), and effective mass (m*) of $ZrSe_2$ monolayer. (a) and (b) are the m* fitting curves of the electrons along x and y directions, respectively. (c) and (d) are the m* fitting curves of the holes along x and y directions, respectively. (e) and (f) are the fitting curves of C along the x and y directions, respectively. (g) and (h) are the fitting curves of E_d along x and y directions, respectively.

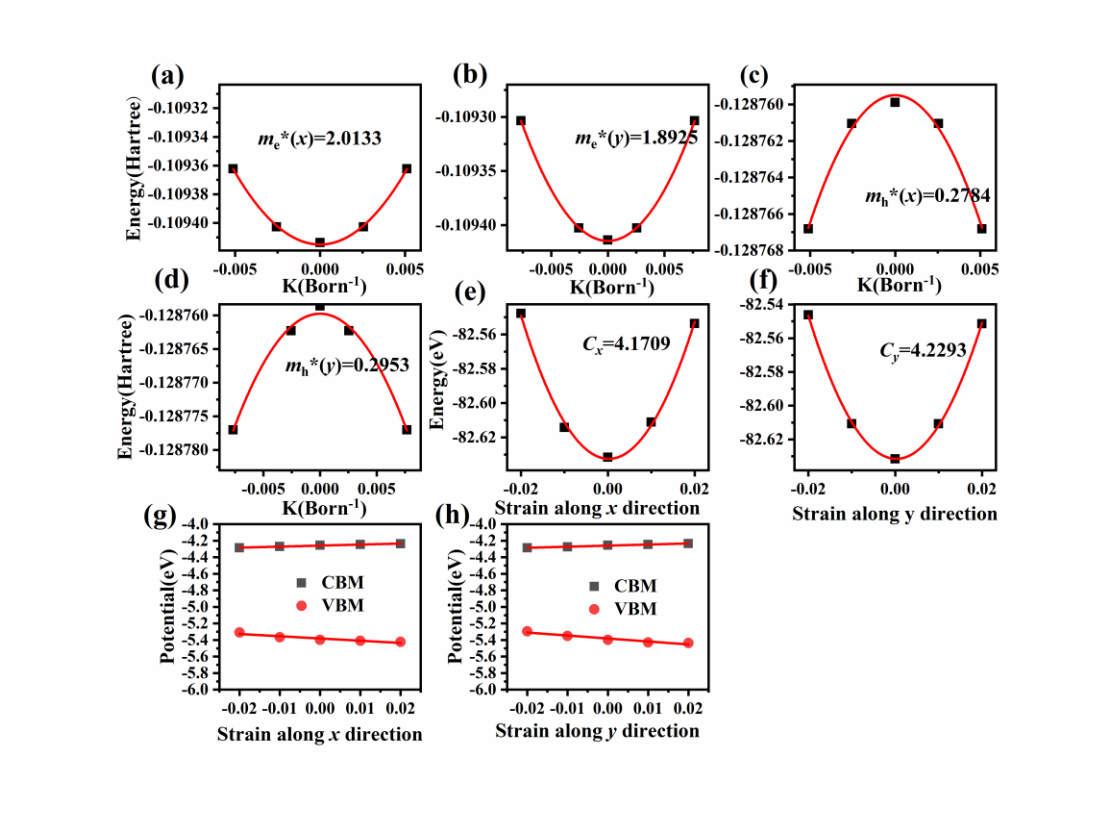

Fig. S8. Fitting curve of elastic constant (C), deformation potential constant (E_d), and effective mass (m^*) of $GaAs_3$ monolayer. (a) and (b) are the m^* fitting curves of the electrons along x and y directions, respectively. (c) and (d) are the m^* fitting curves of the holes along x and y directions, respectively. (e) and (f) are the fitting curves of C along the x and y directions, respectively. (g) and (h) are the fitting curves of E_d along x and y directions, respectively.

Table S2. The elastic modulus (C), deformation potential constant (E_d), effective mass (m^*) and carrier mobility (μ) for the $HfSe_2$, $ZrSe_2$, and $GaAs_3$ monolayers along with the x and y directions at 300 K.

Monolayer	Direction	Carrier	C (N/m)	E_d (eV)	m^* (m_0)	μ ($cm^2V^{-1}s^{-1}$)
$HfSe_2$	x	electron	107.60	0.86	0.24	36992.92
		hole	107.60	2.10	0.35	2907.25
	y	electron	103.16	1.29	0.29	10549.15
		hole	103.16	9.39	0.32	161.24
$ZrSe_2$	x	electron	109.48	1.88	0.27	6126.36
		hole	109.48	3.45	0.42	727.58
	y	electron	98.88	1.40	0.33	6736.70
		hole	98.88	9.80	0.28	182.21
$GaAs_3$	x	electron	68.28	1.23	0.25	10196.95
		hole	68.28	2.71	0.26	7896.72
	y	electron	67.52	1.31	1.80	193.81
		hole	67.52	3.59	1.69	26.02

3. Calculational details for the optical properties and the solar-to-hydrogen conversion efficiency (η'_{STH})

The equation of optical absorption coefficient $\alpha(\omega)$ is [12,13]

$$\alpha(\omega) = \sqrt{2}\sqrt{\sqrt{\varepsilon_r^2(\omega) + \varepsilon_i^2}(\omega) - \varepsilon_r(\omega)} \quad (2)$$

Where $\varepsilon_i(\omega)$ is the imaginary part of the complex dielectric function $\varepsilon(\omega) = \varepsilon_r(\omega) + i\varepsilon_i(w)$, can be calculated by the following equation [14]:

$$\varepsilon_i(\omega) = \frac{4\pi^2}{m^2\omega^2}\Sigma_{c,v}\int_{Bz}\frac{2}{(2\pi)^3}\left|M_{c,v}(k)\right|^2\delta(\varepsilon_{ck} - \varepsilon_{vk} - h_\omega)d^3k \quad (3)$$

Where $\left|M_{c,v}(k)\right|^2$ represent the momentum matrix element, c and v represent the conduction and valence band states, respectively. $\varepsilon_i(\omega)$ can be calculated by VASP. The real part $\varepsilon_r(\omega)$ can be calculated from the imaginary part $\varepsilon_i(\omega)$ of the complex dielectric function by using the Kramer-Kroning relationship [15].

The solar-to-hydrogen conversion efficiency (η_{STH}) and solar-to-fuel (η_{STF}) conversion efficiency is the result of the efficiency of light absorption η_{abs} and the efficiency of carrier utilization η_{cu}, which can be considered as the crucial factor in determining the catalytic ability of photocatalysts. We calculated $\eta_{\mathrm{STH/STF}}$, η_{abs}, and η_{cu} based on the following formula [16]:

$$\eta_{\mathrm{STH/STF}} = \eta_{\mathrm{abs}} \times \eta_{\mathrm{cu}} \tag{4}$$

$$\eta_{\mathrm{abs}} = \frac{\int_{E_{\mathrm{g}}}^{\infty} P(h\omega)\, d(h\omega)}{\int_{0}^{\infty} P(h\omega)\, d(h\omega)} \tag{5}$$

$$\eta_{\mathrm{cu}} = \frac{\Delta G \int_{E}^{\infty} \frac{P(h\omega)}{h\omega} d(h\omega)}{\int_{E_{\mathrm{g}}}^{\infty} P(h\omega)\, d(h\omega)} \tag{6}$$

$$E = \begin{cases} E_{\mathrm{g}},\ (\chi(\mathrm{H_2}) \geq 0.2, \chi(\mathrm{O_2}) \geq 0.6) \\ E_{\mathrm{g}} + 0.2 - \chi(\mathrm{H_2}), (\chi(\mathrm{H_2}) < 0.2, \chi(\mathrm{O_2}) \geq 0.6) \\ E_{\mathrm{g}} + 0.6 - \chi(\mathrm{O_2}), (\chi(\mathrm{H_2}) \geq 0.2, \chi(\mathrm{O_2}) < 0.6) \\ E_{\mathrm{g}} + 0.8 - \chi(\mathrm{H_2}) - \chi(\mathrm{O_2}), (\chi(\mathrm{H_2}) < 0.2, \chi(\mathrm{O_2}) < 0.6) \end{cases} \tag{7}$$

Where $P(h\omega)$ is the AM1.5G solar energy flux at the photo energy $h\omega$; E_g(HSE) is the bandgap of the layer materials; $\chi(\mathrm{H_2})$ and $\chi(\mathrm{O_2})$ are the overpotentials for hydrogen and oxygen evolution reactions, respectively. ΔG represents the potential difference of 1.23 eV for water splitting or 1.06 eV for CO_2 conversion into CH_4 using H_2O as electron donor, and E is the energy of photons that can actually be utilized for water splitting.

Because the intrinsic electric field would promote the electron-hole separation, so the corrected STH/STF efficiency ($\eta'_{\mathrm{STH/STF}}$) for polarized materials in photocatalytic water splitting reaction can be calculated as:

$$\eta'_{\mathrm{STH/STF}} = \eta_{\mathrm{STH/STF}} \times \frac{\int_{0}^{\infty} P(h\omega)\mathrm{d}(h\omega)}{\int_{0}^{\infty} P(h\omega)\mathrm{d}(h\omega) + \Delta\Phi \int_{0}^{\infty} P(h\omega)\mathrm{d}(h\omega)} \tag{8}$$

Where $\Delta\Phi$ is the vacuum level difference between the two respectively surfaces of the polarized material.

Table S3. The energy conversion efficiency of the light absorption of light (η_{abs}), carrier utilization (η_{cu}), η'_{STH} and η'_{STF} of the $HfSe_2/GaAs_3$ heterostructure.

$HfSe_2/GaAs_3$	$E_{g\text{-}HfSe2}$ (eV)	$E_{g\text{-}GaAs3}$ (eV)	$\chi(H_2)$ (eV)	$\chi(O_2)$ (eV)	$\chi(CO_2)$ (eV)	$\Delta\varphi$ (eV)	η_{abs} (%)	η_{cu} (%)	η'_{STH} (%)	η'_{STF} (%)
-3%	0.96	0.88	0.13	0.19	0.30	0.03	91.31	42.96	38.62	34.99
-2%	1.08	1.00	0.16	0.28	0.33	0.05	84.83	47.36	39.29	33.37
-1%	1.19	1.11	0.20	0.39	0.37	0.06	79.00	52.01	40.54	33.45
0%	1.31	1.23	0.24	0.49	0.41	0.08	73.37	55.35	39.45	32.47
1%	1.39	1.30	0.27	0.56	0.44	0.09	70.23	50.73	39.06	32.00
2%	1.47	1.38	0.29	0.65	0.46	0.10	64.96	58.15	36.65	30.31
3%	1.55	1.39	0.32	0.73	0.49	0.11	60.47	56.44	33.12	27.31
4%	1.63	1.39	0.34	0.82	0.51	0.10	56.51	54.96	30.29	24.71

Table S4. The energy conversion efficiency of the light absorption of light (η_{abs}), carrier utilization (η_{cu}), η'_{STH} and η'_{STF} of the $ZrSe_2/GaAs_3$ heterostructure.

$ZrSe_2/GaAs_3$	$E_{g\text{-}GaAs3}$ (eV)	$E_{g\text{-}ZrSe2}$ (eV)	$\chi(H_2)$ (eV)	$\chi(O_2)$ (eV)	$\chi(CO_2)$ (eV)	$\Delta\varphi$ (eV)	η_{abs} (%)	η_{cu} (%)	η'_{STH} (%)	η'_{STF} (%)
-3%	0.98	0.81	0.15	0.24	0.32	0.05	90.40	46.83	41.10	35.75
-2%	1.09	0.92	0.19	0.33	0.36	0.03	84.51	50.68	42.25	35.38
-1%	1.18	1.02	0.21	0.43	0.38	0.02	80.32	54.55	43.45	35.93
0%	1.30	1.04	0.25	0.52	0.42	0	73.66	57.98	42.71	35.12
1%	1.36	1.21	0.28	0.60	0.45	0	71.35	60.61	43.25	35.85
2%	1.52	1.29	0.45	0.67	0.62	0.02	62.35	57.14	35.42	29.12
3%	1.51	1.36	0.46	0.74	0.63	0.03	62.80	57.31	35.68	29.42
4%	1.60	1.43	0.57	0.81	0.74	0.04	57.77	55.43	31.69	25.91

4.Calculational method of the Gibbs free energy.

The ΔG can be calculated by the following equation [17-20]:

$$\Delta G = \Delta E - T\Delta S - \Delta E_{\mathrm{ZPE}} \quad (9)$$

Where ΔE, ΔE_{ZPE} and ΔS represent the differences in total energy, zero-point energy and entropy of the slab with and without adsorbed intermediates. T is the temperature 298K. The E_{ZPE} can be calculated by $E_{\mathrm{ZPE}} = \frac{1}{2}\Sigma\hbar\nu$, where the ν is the vibrational frequency over normal modes, and the zero-point of slab can be negligible. The entropies of the free molecules were taken from the standard tables in Physical chemistry and that of intermediates were obtained from vibrational frequency. For those reactions involving the release of protons and electrons, the free energy of one pair of proton and electron (H^+/e^-) was taken as $1/2G_{H2}$.

In the aqueous solution, the HER with two electrons pathway, which can be written as:

$$* + H^+ + e^- \rightarrow *H$$

$$*H + H^+ + e^- \rightarrow * + H_2$$

The OER process can be written as:

$$H_2O + * \rightarrow *OH + H^+ + e^-$$

$$*OH \rightarrow *O + H^+ + e^-$$

$$*O + H_2O \rightarrow *OOH + H^+ + e^-$$

$$*OOH \rightarrow * + O_2 + H^+ + e^-$$

The CO_2RR process with eight-electron pathway which can be written as:

$$* + CO_2 + e^- + H^+ \rightarrow *OOCH$$

$$*OOCH + e^- + H^+ \rightarrow *OCHOH\ (* + CO + H_2O\ /\ * + HCOOH)$$

$$*OCHOH + H^+ + e^- \rightarrow *OCH_2OH\ (*OCH + H_2O)$$

$$*OCH_2OH + H^+ + e^- \rightarrow *OCH_2 + H_2O$$

$$*OCH_2 + H^+ + e^- \rightarrow *OCH_3$$

$$*OCH_3 + H^+ + e^- \rightarrow *O + CH_4\ (* + CH_3OH\ /\ *OHCH_3)$$

$$*O + H^+ + e^- \rightarrow *OH$$

$$*OH + H^+ + e^- \rightarrow * + H_2O$$

Table. S5 The calculated total energies of the *H, *OOCH, and *COOH absorbed on Ga or As atoms of $HfSe_2/GaAs_3$ and $ZrSe_2/GaAs_3$ heterostructures optimized by the *k*-points of 1×1×1.

	Intermediates	energy		Intermediates	energy
$HfSe_2/GaAs_3$	*H(Ga)	-533.4396	$ZrSe_2/GaAs_3$	*H(Ga)	-467.2749
	*H(As)	-533.5221		*H(As)	-467.3630
	*OOCH(Ga)	-557.5166		*OOCH(Ga)	-491.2834
	*COOH(Ga)	-556.7326		*COOH(Ga)	-490.4588
	*OOCH(As)	-556.3622		*OOCH(As)	-490.2043
	*COOH(As)	-556.5328		*COOH(As)	-490.2940

Table. S5 The calculated ZPE, TS, and the Δ*G*s for the adsorbed molecules of $HfSe_2/GaAs_3$ configuration.

$HfSe_2/GaAs_3$	ZPE (eV)	TS (eV)	Δ*G*(eV)
*OH(OER)	0.3172	0.1081	2.3506
*O(OER)	0.0594	0.0872	1.0456
*OOH(OER)	0.4292	0.1519	2.0967
*H	0.1903	0.0168	0.3530
*COOH	0.6105	0.2354	0.6292
*OOCH	0.6145	0.2427	-0.1523
*OCHOH	0.9115	0.1889	0.4301
*OCH	0.4969	0.1064	0.5351
CO	0.1330	0.6110	0.5433
HCOOH	0.8860	0.7690	0.4463
$*OCH_2OH$	1.2367	0.2354	0.1598
$*OCH_2$	0.7799	0.1604	-0.3483
$*OCH_3$	1.0851	0.0962	-0.1849
$*OHCH_3$	1.4083	0.1323	-0.3971
CH_3OH	1.3450	0.7410	-0.1519
$*O(CO_2RR)$	0.0759	0.0400	-0.7286
$*OH(CO_2RR)$	0.3329	0.1519	-0.4862

Table. S6 The calculated ZPE, TS, and the Δ*G*s for the adsorbed molecules of $ZrSe_2/GaAs_3$ configuration.

$ZrSe_2/GaAs_3$	ZPE (eV)	TS (eV)	Δ*G*(eV)
*OH(OER)	0.3210	0.1125	2.2163
*O(OER)	0.0576	0.0957	1.0513
*OOH(OER)	0.4307	0.1500	2.1662
*H	0.1898	0.0173	0.2653
*COOH	0.6096	0.2326	0.7015
*OOCH	0.6095	0.2418	-0.1044
*OCHOH	0.9214	0.2188	0.3821
*OCH	0.4981	0.1046	0.5175
CO	0.1330	0.6110	0.4953
HCOOH	0.8860	0.7690	0.3983
$*OCH_2OH$	1.2065	0.1806	0.3600
$*OCH_2$	0.7466	0.1233	-0.4243
$*OCH_3$	1.0850	0.1596	-0.3218
CH_3OH	1.3450	0.7410	-0.1237
$*OHCH_3$	1.4177	0.2142	-0.4270
$*O(CO_2RR)$	0.0756	0.0493	-0.7089
$*OH(CO_2RR)$	0.3268	0.0997	-0.3894

References

[1] E. Aretouli, P. Tsipas, D. Tsoutsou. Two-dimensional semiconductor $HfSe_2$ and $MoSe_2/HfSe_2$ van der Waals heterostructures by molecular beam epitaxy. *Appl. Phys. Lett*, 2015, **106**(14), 143105.

[2] Q. Zhao, Y. Guo, K. Si, Z. Ren, J. Bai, X. Xu. Elastic, electronic, and dielectric properties of bulk and monolayer ZrS_2, $ZrSe_2$, HfS_2, $HfSe_2$ from van der Waals density-functional theory. *Phys. Status. Solidi. B*, 2017, **254**(9), 1700033.

[3] M. J. Mleczko, C. Zhang, H. R. Lee, $HfSe_2$ and $ZrSe_2$: Two-dimensional semiconductors with native high-*κ* oxides. *Sci. Adv*, 2017, **3**(8), e1700481.

[4] K. Terashima, I. Imai. Indirect absorption edge of ZrS_2 and HfS_2. *Solid. State. Commun*, 1987, **63**(4), 315.

[5] Y. Tian, M. Y. Zheng, Y. Cheng, Z. G. Yin, J. Jiang, G. k. Wang, J. R. Chen, X. X. Li, J. Qi and X. W. Zhang. Epitaxial growth of $ZrSe_2$ nanosheets on sapphire via chemical vapor deposition for optoelectronic application. *J. Mater. Chem. C*, 2021, **9**(39), 13954.

[6] R. A. B. Villaos, H. N. Cruzado, J. S. C. Dizon, A. B. Maghirang, Z. Q. Huang, C. H. Hsu, S. M. Huang, H. Lin and F. C. Chuang. Evolution of the electronic properties of ZrX_2 (X= S, Se or Te) thin films under varying thickness. *J. Phys. Chem. C*. 2021, **125**(1), 1134–1142.

[7] M. Abdulsalam and D. P. Joubert, Optical spectrum and excitons in bulk and monolayer MX_2 (M= Zr, Hf; X= S, Se). *Phys. Status. Solidi B*, 2016,**253**(4), 705–711.

[8] J. Bardeen, W. Shockley. Deformation potentials and mobilities in nonpolar crystals. *Phys. Rev*, 1950, **80**(1), 72.

[9] S. Bruzzone, G. Fiori. *Ab initio* simulations of deformation potentials and electron mobility in chemically modified graphene and two-dimensional hexagonal boron-nitride. *Appl. Phys. Lett*, 2011, **99**(22), 222108.

[10]J. Chen, J. Xi, D. Wang, Z. Shuai. Carrier mobility in graphene should be even larger than that in graphene: a theoretical prediction. *J. Phys. Chem. Lett*, 2013, **4**(9), 1443-1448.

[11]J. Dai, X. C. Zeng. Titanium trisulfide monolayer: theoretical prediction of a new direct gap semiconductor with high and anisotropic carrier mobility. *Angew Chem*,

2015, **127**(26), 7682-7686.

[12] X. Zhang, X. Zhao, D. Wu, Y. Jing, Z. Zhou. $MnPSe_3$ monolayer: A promising 2D visible light photo hydrolytic catalyst with high carrier mobility. *Adv. Sci*, 2016, **3**(10), 1600062.

[13] S. Saha, T. P. Sinha, A. Mookerjee. Electronic structure, chemical bonding, and optical properties of paraelectric $BaTiO_3$. *Phys. Rev. B*, 2000, **62**(13), 8828-8834.

[14] P. Li, C. W. Zhang, J. Lian, M. J. Ren, P. J. Wang, X. H. Yu, S. Gao. First-principal study of optical properties of Cu-doped CdS. *Opt. Commun,* 2013, **295**, 45-52.

[15] Y. Li, Z. Chen. Tuning electronic properties of germanane layers by external electric field and biaxial tensile strain: a computational study. *J. Phys. Chem. C*, 2014, **118**(2),1148.

[16] C. F. Fu, J. Y. Sun, Q. Q. Luo, X. X. Li, W. Hu, J. L. Yang. Intrinsic electric fields in two-dimensional materials boost the solar-to-hydrogen efficiency for photocatalytic water splitting. *Nano Lett*, 2018, **18**(10), 6312-6317.

[17] G. Gao, A. P. O'Mullane, A. Du. 2D MXenes: a new family of promising catalysts for the hydrogen evolution reaction. *ACS Catal*, 2017, **7**(1), 494.

[18] T. He, G. Gao, L. Kou, G. Will, A. Du, Endohedral metallofullerenes (M@C60) as efficient catalysts for highly active hydrogen evolution reaction. *J Catal*, 2017, **351**, 231.

[19] D. Er, H. Ye, N. C. Frey, H. Kumar, J. Lou, V. B. Shenoy, Prediction of enhanced catalytic activity for hydrogen evolution reaction in Janus transition metal

dichalcogenides. *Nano Lett*, 2018, **18**(6), 3943,18.

[20]C. Ling, L. Shi, Y. Ouyang, X. C. Zeng, J. Wang, Nanosheet supported single-metal atom bifunctional catalyst for overall water splitting. *Nano Lett*, 2017, **17**(8), 5133.